Conformational Analysis of a Tetrasaccharide Based on NMR Spectroscopy and Molecular Dynamics Simulations

Clas Landersjö,[†] Jennie L. M. Jansson,[†,‡] Arnold Maliniak,[‡] and Göran Widmalm*[,†]

Department of Organic Chemistry and Division of Physical Chemistry, Arrhenius Laboratory, Stockholm University, S-106 91 Stockholm, Sweden

Received: April 28, 2005; In Final Form: June 13, 2005

The conformational preference of the human milk oligosaccharide lacto-*N*-neotetraose, β-D-Gal*p*-(1 → 4)-β-D-Glc*p*NAc−(1 → 3)-β-D-Gal*p*-(1 → 4)-D-Glc*p*, has been analyzed using ^{1}H,^{1}H T-ROESY and ^{1}H,^{13}C *trans*-glycosidic *J* coupling experiments in isotropic solution and ^{1}H,^{13}C residual dipolar couplings (RDCs) obtained in lyotropic liquid crystalline media. Molecular dynamics simulations of the tetrasaccharide with explicit water as the solvent revealed that two conformational states are significantly populated at the ψ glycosidic torsion angle, defined by $C_{anomeric}$−O−C−H, of the (1 → 3)-linkage. Calculation of order parameters, related to the molecular shape, were based on the inertia tensor and fitting of experimental RDCs to different conformational states showed that $\psi^+ > 0°$ is the major and $\psi^- < 0°$ is the minor conformation in solution, in complete agreement with a two-state analysis based on the T-ROESY data. Attention was also given to the effect of salt (200 mM NaCl) in the anisotropic medium, which was a ternary mixture of *n*-octyl-penta-(ethylene glycol), *n*-octanol, and D_2O.

Introduction

Analysis of molecular conformation and the inherent dynamics is a prerequisite for the understanding of molecular interactions and biochemical processes. NMR spectroscopy has been the paramount tool for several decades, employing in particular the nuclear Overhauser effect (NOE) and spin−spin coupling constants (*J*) to derive the configuration as well as conformation of molecules. For many years, nuclear dipolar interactions have been used in the analysis of molecular structure in classical thermotropic and lyotropic liquid crystalline phases or solutes dissolved therein.[1] More recently, NMR residual dipolar couplings (RDCs) obtained in magnetic field oriented media[2] have found use in the determination of biomolecular structures[3] such as proteins, nucleic acids, and carbohydrates as well as in interaction studies.[4] Furthermore, there is a continuous development of anisotropic media that can be aligned either mechanically or magnetically, with increased pH and temperature ranges compared to those currently available.[5] Likewise, there is rapid progress in the area of NMR pulse sequences for measurements of various types of RDCs.[6−8] Finally, new and more sophisticated tools employed for interpretation of dipolar couplings are being developed.[9−12]

In structural analysis based on RDCs, the use of several orienting media results in a range of alignment tensors, which provide independent structural information.[13−16] However, for this procedure to work properly it is important that the molecular conformation (or the equilibrium between conformers) is not significantly altered between the media. A problem that may occur is that the solute interacts too strongly with the aligning aggregates, for example, in the case of charged species, a phenomenon that may be reduced with the presence of a sufficiently high salt concentration in the medium.[17,18] Thus, it is of great importance to understand the properties of different alignment media and to clarify possible conformational changes in the studied solute molecules.

The information from ^{1}H, ^{1}H NOEs, and *trans*-glycosidic *J* couplings in oligosaccharides is strongly limited because usually only one or two NOEs are observed across a glycosidic linkage. In addition, each one of the pertinent heteronuclear three-bond *J* couplings is consistent with up to four possible conformations. Therefore, the use of RDCs provides a valuable addition in the determination of carbohydrate conformation and dynamics. Several reports on the subject have been published utilizing ^{1}H,^{13}C and ^{1}H,^{1}H RDCs obtained in different ordering media.[19−24]

Human milk is composed of more than 100 lactose-derived oligosaccharides[25] known to act as potent inhibitors of bacterial adhesion to epithelial surfaces. Therefore, oligosaccharides of this type can be thought of as soluble receptors that have the ability to inhibit the initial stage of an infective process. We[26,27] and others[28−32] have studied some of these carbohydrates by obtaining RDCs, which were used subsequently in conformational analysis. In the present study we extend our analysis of lacto-*N*-neotetraose (LNnT) (Figure 1), an oligosaccharide structure that also has been described in the context of molecular mimicry[33] for pathogenic bacteria and glycolipids present on human cells. The NMR techniques utilized herein were ^{1}H,^{1}H T-ROESY, *trans*-glycosidic $^3J_{C,H}$, together with ^{1}H,^{13}C and ^{1}H,^{1}H RDCs measured in the anisotropic medium *n*-octyl-penta-(ethylene glycol) referred to as C8E5, *n*-octanol, and D_2O.[34] This lyotropic liquid crystalline phase has been shown to tolerate higher salt concentrations,[35] a property of particular interest in regard to our previous conformational studies of LNnT.

Materials and Methods

General. Lacto-*N*-neotetraose was obtained from IsoSep AB (Tullinge, Sweden). The materials for the dilute liquid crystal solution, *n*-octyl-penta(ethylene glycol) (C8E5) and *n*-octanol,

* Corresponding author. E-mail: gw@organ.su.se.
† Department of Organic Chemistry.
‡ Division of Physical Chemistry.

10.1021/jp052206y CCC: $30.25
Published on Web 08/19/2005

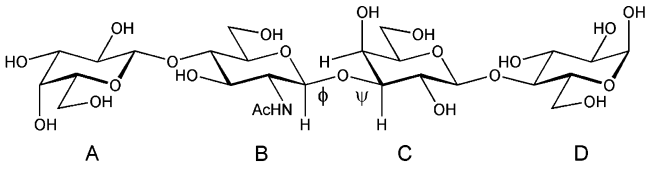

Figure 1. Schematic of the tetrasaccharide lacto-*N*-neotetraose β-D-Gal*p*-(1 → 4)-β-D-Glc*p*NAc−(1 → 3)-β-D-Gal*p*-(1 → 4)-α-D-Glc*p* (LNnT) where the torsion angles at glycosidic (1 → 3)-linkage are denoted by ϕ and ψ. Sugar residues are labeled A through D, starting from the terminal nonreducing end. In the text a subscript (ϕ_i, ψ_i where i = A, B, C) is used to refer to the pertinent glycosidic torsion angle.

were purchased from Sigma (St. Louis, MO) and Fluka (Buchs, Switzerland), respectively. Sodium chloride was obtained from Merck (Darmstadt, Germany). All of the chemicals had a purity >99% and were used as delivered.

NMR Spectroscopy. The NMR experiments were carried out in D_2O on a 600-MHz Varian Inova spectrometer equipped with a 5-mm PFG triple-resonance probe. Proton−proton cross-relaxation rates in LNnT (15 mM) were measured at 20 °C using 1D ^{1}H,^{1}H DPFGSE T-ROESY experiments as described previously.[36] Selective ^{13}C excitation of the C3 resonance from residue C of LNnT (57 mM, Shigemi tube BMS-005TV, Shigemi, Allison Park, PA) followed by evolution of the long-range coupling to H1 in residue B was used to obtain the *trans*-glycosidic $^3J_{H,C}$ value employing the previously described pulsed field gradient version of the experiment.[37]

The dilute liquid crystal solutions were prepared by dissolving C8E5 (5% w/v) in D_2O, followed by addition of *n*-octanol to a final C8E5/*n*-octanol ratio of 0.87. When the lyotropic phase is formed after vigorous shaking, a light blue, transparent, non-viscous solution appears. This lyotropic phase tolerates the addition of up to 500 mM NaCl. The homogeneity of the preparation was checked in the NMR spectrometer by the ^{2}H quadrupolar splitting of D_2O prior to the addition of LNnT (7 mg in 700 μL, 14 mM). The resulting ^{2}H quadrupolar splitting was 39.4 and 38.9 Hz (200 mM NaCl).

Proton−carbon residual dipolar couplings (D_{CH}) were obtained in both the absence and presence of 200 mM NaCl at 15 °C as the difference between the one-bond ^{1}H,^{13}C splitting measured in the ordered phase and the isotropic phase. Because of spectral overlap and the parallel nature of several of the ring C−H vectors, about half of the resonances were selected for evaluation. A slightly modified *J*-modulated constant-time HSQC experiment[38] was used with only the final gradient in the reverse INEPT part of the pulse sequence. In total, 6−7 experiments with 2($T - \Delta$) values between 24.5 and 28.0 ms were carried out for ∼6 h/experiment (isotropic phase) and ∼10 h/experiment (ordered phase). Each spectrum consisted of 2048 × 128 complex data points with 48−96 transients/t_1-increment and spectral widths of 2500 and 8800 Hz in the F2 and F1 dimensions, respectively. The FIDs were zero-filled to 16 384 × 2048 complex points and multiplied with a Gaussian weighting function prior to the Fourier transformation. Cross-peak integration was performed using the same integration limits in all spectra. The couplings were obtained by fitting the cross-peak intensities from a series of experiments with different 2($T - \Delta$) values to $C \times \cos[2 \times {}^1J_{C,H} (T - \Delta)]$ in KaleidaGraph (Synergy Software, Reading, PA). The error in each measured coupling was estimated using the jackknife procedure,[39,40] and the error in the RDC was calculated as the propagated error.[41]

Proton−proton scalar ($^3J_{H,H}$) and residual dipolar couplings (D_{HH}) of LNnT were extracted from phase-sensitive COSY spectra using the NMRPipe[42] based fitting program, Amplitude-Constrained Multiple Evaluation (ACME).[43] From the splittings in the spectra recorded at 30 °C, J and $J + 2D$ were obtained for LNnT in the isotropic phase (9 mM in D_2O) and in the ordered phase (6 mM) using cetylpyridinium chloride/*n*-hexanol/brine (200 mM NaCl in D_2O) as described by Lycknert et al.[23] The resulting ^{2}H quadrupolar splitting was 6.7 Hz. In the experiments, 40 and 96 transients were acquired for each of the 128 t_1-increments in the two phases, respectively, using a relaxation delay between the scans of >5 T_1.

Molecular Simulations. For the molecular dynamics (MD) simulations, CHARMM[44] (parallel version, C27b4) software was used employing a CHARMM22 type of force field[45] modified for carbohydrates and referred to as PARM22/SU01.[46] Initial conditions were prepared by placing the tetrasaccharide LNnT in a previously equilibrated cubic water box of length 40.39 Å containing 2197 modified TIP3P water[47] molecules and removing the solvent molecules that were closer than 2.5 Å to any solute atom. This procedure resulted in a system with LNnT and 2129 water molecules. Energy minimization was performed with Steepest Descent, 200 steps, followed by Adopted Basis Newton−Raphson until the root-mean-square gradient was less than 0.01 kcal mol^{-1} Å^{-1}. The simulation was carried out with the leap-frog algorithm,[48] a dielectric constant of unity, a time step of 2 fs, and data were saved every 0.2 ps for analysis. SHAKE was used to restrain hydrogen-heavy atom bonds[49] with a tolerance gradient of 10^{-4}. Initial velocities were assigned at 103 K, followed by heating with 5 K increments during 8 ps to 303 K, where the system was equilibrated for 200 ps. The production run was performed for 4 ns with the temperature scaled by Berendsen's weak coupling algorithm.[50] Periodic boundary conditions and the minimum image convention were used together with a heuristic nonbond frequency update and a force shift cutoff[51] acting to 12 Å. For specific analyses, the ψ_B^+ conformational state was described as the 0.3−0.8 ns part and the ψ_B^- conformational state as the 3.0−3.5 ns of the trajectory. For calculation of S_Ω^2, the C4A−C1D and O3C−H1B vectors in the former case and the C4A−C1D and C1B−H1B vectors in the latter case were chosen for the reference system and the values of S_Ω^2 were obtained from the long time decay of the autocorrelation function.

Simulations were performed on an IBM SP2 computer at the Center for Parallel Computers, KTH, Stockholm, using 16 nodes that resulted in a CPU time of approximately 120 h/ns.

Results and Discussion

Prior to the extended RDC analysis, any possible conformational difference in LNnT as a result of increased ionic strength was investigated in isotropic media (D_2O and D_2O/200 mM NaCl). Guided by our previous investigation,[27] we focus on the conformations related to the glycosidic linkage between residues B and C. The reason is that this region of the molecule exhibits the most pronounced conformational transitions. The 1D ^{1}H,^{1}H T-ROESY experiment[36] was utilized with selective excitation of the resonance from H4 in C. The T-ROESY spin-lock is particularly powerful in that there is almost complete elimination of TOCSY magnetization transfer, even when the RF transmitter is positioned in the spectral region of interest.[52] The cross-relaxation rates from H4 in C to H1 in B (σ = 0.026 and 0.028 s^{-1} in water and brine, respectively) were related to the effective distances using the isolated spin-pair approximation (ISPA) with H4B to both H3B and H5B (overlapping, σ = 0.40 and 0.36 s^{-1} in water and brine, respectively) as the internal distance (2.41 Å). These results correspond to $r_{H1B,H4C}$ = 3.4 Å in water and $r_{H1B,H4C}$ = 3.3 Å in brine solution. However, this difference in experimental distance is too small to support any conforma-

TABLE 1: Averages Calculated from the Trajectory Generated in the MD Simulation of LNnT

torsion angle (deg)[a]		$^3J_{C,H}$ (Hz)[b]		proton distance (Å)[c]	
ϕ_A	48 (15)	J_{ϕ_A}	2.8	H1A−H4B	2.32
ψ_A	−3 (17)	J_{ψ_A}	6.1	H1B−H3C	2.35
ϕ_B	41 (14)	J_{ϕ_B}	3.7	H1B−H4C	2.96
ψ_B	−17 (42)	J_{ψ_B}	3.5	H1C−H4D	2.28
ϕ_C	43 (14)	J_{ϕ_C}	3.3	H4C−H3C	2.41
ψ_C	−9 (19)	J_{ψ_C}	5.9	H4C−H5C	2.41

[a] Root-mean-square deviations in parentheses. [b] Derived from the Karplus-type relationship.[54] [c] $1/r = \langle r^{-6}\rangle^{1/6}$.

tional change in LNnT in the two solutions. It should be noted that severe proton spectral overlap is present in LNnT, even at 800 MHz, which precludes straightforward interpretation of 2D ^{1}H,^{1}H NOESY build-up data into precise cross-relaxation rates and subsequently interproton distances (data not shown). In addition, the *trans*-glycosidic heteronuclear coupling constant related to the ϕ_B torsion angle was measured in D_2O by selective excitation of the resonance from C3 in residue C of LNnT, which yielded $J_{H1B,C3C} = 4.1 \pm 0.1$ Hz.

Molecular dynamics (MD) simulations of LNnT were performed in the isotropic phase with explicit water as the solvent. A modified CHARMM force field referred to as PARM22/SU01 was employed[46] in the 4-ns simulation. Selected averages from the MD simulation are compiled in Table 1. The averages for the ϕ glycosidic torsion angles are very similar, as anticipated for this linear tetrasaccharide consisting of β-D-Hexopyranosyl residues, that is, the conformation is governed by stereoelectronic interactions known as the exo-anomeric effect.[53] All three ψ glycosidic torsion angles show comparable values. However, the root-mean-square deviation (rmsd) for the ψ_B torsion angle is ~3 times higher than for any of the other glycosidic torsions, revealing significant flexibility at the β-(1 → 3)-linkage. From the MD simulation, we calculated parameters that can be compared to those determined experimentally by NMR spectroscopy. Heteronuclear $^3J_{H,C}$ across the glycosidic linkage can be analyzed using a Karplus-type relationship.[54] The simulation showed $J_{H1B,C3C} = 3.7$ Hz, which is in good agreement with that observed experimentally (vide infra), thereby lending credence to the conformation at the ϕ_B glycosidic torsion angle. Although the rmsd of ϕ_B is relatively low, that of J_{ϕ_B} is quite high (rmsd = 1.5 Hz) because the torsion angle populates a conformational region in which the Karplus-curve is steep. In light of this, the close resemblance of the simulated and the experimentally observed J_{ϕ_B} is encouraging.

The proton−proton distance H1B−H4C is an important marker of conformational preference at the central glycosidic torsion angle. Analysis of the trajectory indicates clearly two distinct conformational regions (Figure 2b). Both the H1B−H3C and H1B−H4C distances correlate well with conformational changes of ψ_B (Figure 2). The MD trajectory was also analyzed with respect to the two conformational states at ψ_B, denoted as ψ_B^+ and ψ_B^- referring to the sign of the torsional angle, that is, in the former $\psi_B > 0°$ and in the latter $\psi_B < 0°$. Both states are sampled several times. However, the number of transitions is still few and precludes a statistically meaningful analysis.[55] The torsion angles in these states correspond to $\langle\psi_B^+\rangle = 40°$ and $\langle\psi_B^-\rangle = -43°$ (Figure 3). The MD simulation showed 32% of ψ_B^+ and 68% of ψ_B^-, favoring the latter to some extent. It should be noted that because the number of transitions are few the error in the populations is relatively large and a significantly longer simulation would be needed to alleviate this uncertainty.[56] From the MD simulation we conclude, therefore, that the two conformational states of ψ_B are significantly

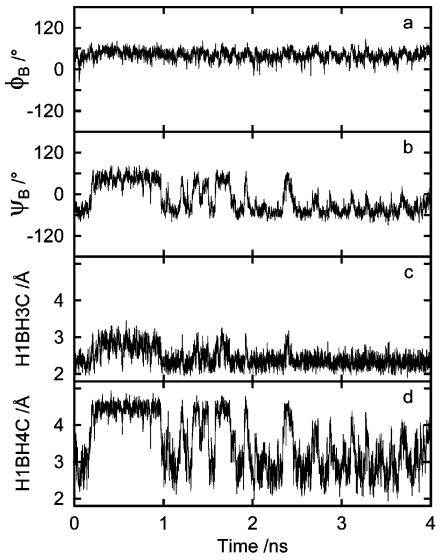

Figure 2. The time dependence of the glycosidic torsion angles ϕ_B, ψ_B (a, b) of LNnT and selected inter-residue proton−proton distances (c, d), where the two conformational states are identified according to $\psi_B > 0°$ and $\psi_B < 0°$.

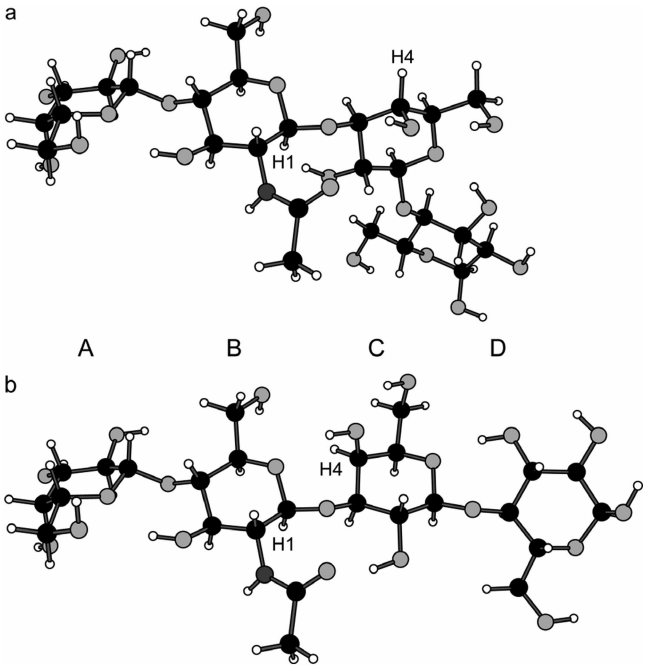

Figure 3. Molecular model of LNnT indicating the flexibility at the glycosidic torsion angle ψ_B, as a result of two significantly populated conformational states: (a) $\langle\psi_B^+\rangle = 40°$ and (b) $\langle\psi_B^-\rangle = -43°$. The distance between H1B and H4C protons (annotated) is sensitive to the conformation at the central glycosidic linkage.

populated, whereas ϕ_B remains essentially constant (Figure 2a) during the entire trajectory.

The effective distance calculated from the full trajectory of the MD simulation for $\langle r_{H1B,H4C}\rangle = 2.96$ Å is slightly shorter than that estimated from experiment (vide supra). The proton−proton distance averaged over 500 ps for each of the conformational states ψ_B^+ and ψ_B^- led to $\langle r_{H1B,H4C}\rangle = 4.45$ and 2.76 Å, respectively. The experimental data together with proton−proton distances from the MD simulation may then be used in a two state analysis:$(1 - x)\langle r_{neg}^{-6}\rangle + (x)\langle r_{pos}^{-6}\rangle = r_{exp}^{-6}$, where x is the fraction that populates the ψ_B^+ conformational state. This gives $x = 0.75$ in water and $x = 0.68$ in brine solution. Thus, the ψ_B^+ conformation is favored by $\Delta G \approx 0.5$ kcal/mol in solution

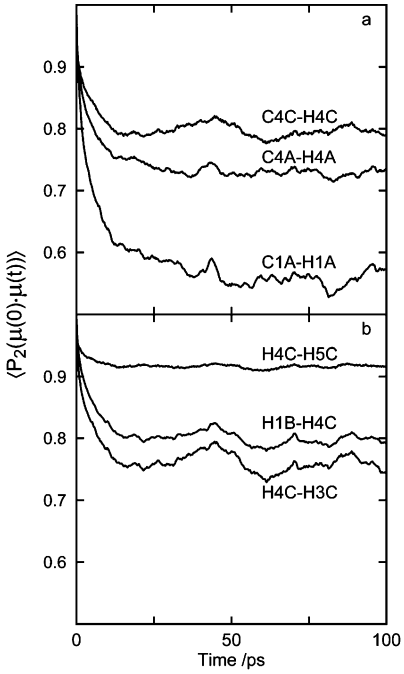

Figure 4. Reorientational correlation functions for LNnT, in which the overall rotation has been removed, calculated for CH vectors (a) and HH vectors (b).

experiments, whereas the ψ_B^- state predominates in the MD simulation and is preferred by approximately an equal free energy difference.

For the ISPA to work properly, the dynamics should be similar for the reference distance and the unknown distance. This can be investigated from an analysis of the MD simulation. We refrain from a detailed dynamic analysis of the complex molecular motions, but in Figure 4 it can be noted that the initial decay of the correlation functions is similar. It seems that these motions are more rapid than expected, but this can be attributed to the well-known properties of the water model used in the simulation, a phenomenon investigated previously.[57] Furthermore, the molecular flexibility may be quantified using a Lipari−Szabo type of order parameter denoted S^2, which for a rigid molecular fragment is unity and becomes zero for completely unrestricted motion.[58] For reasonably rigid molecules, S^2 can be factorized[59] according to

$$S^2 = S^2_{\text{radial}} S^2_{\Omega} \text{ with } S^2_{\text{radial}} = \langle r^{-3}\rangle^2/\langle r^{-6}\rangle \text{ and } S^2_{\Omega} = \lim_{t\to\infty}\langle P_2(\mu(0)\,\mu(t))\rangle$$

where $P_2(x)$ is the second-order Legendre polynomial and $\mu(t)$ defines the orientation of the investigated unit vector in the molecular frame. The ψ_B^+ conformational state is, inter alia, present early in the simulation for ∼500 ps, and the ψ_B^- state can likewise be identified in the latter part of the simulation. We first analyze S^2 for the ψ_B^+ conformational state as the plateau of the reorientational correlation function $\langle P_2(\mu(0)\,\mu(t))\rangle$ where the overall rotation has been removed. Representative CH vectors are shown in Figure 4a, and S^2 values are given in Table 2. The outer sugar residues have lower S^2 values than the two central residues. Also, CH vectors closely parallel to the principal axis of the molecule show higher S^2 values, as anticipated for a molecule like LNnT, which should have a prolate molecular shape.[60] For the proton pairs, the *trans*-glycosidic S^2_{radial} values are close to unity and S^2_{Ω} are similar as seen in Figure 4b and Table 2. Consequently, the proton−proton interactions show similar behavior and may therefore be treated as effective distances. In the ψ_B^- state, a single conformation is more difficult to define, where a few rapidly interconverting substates may be identified. However, the lower S^2 values for the ψ_B^- state follow similar trends (data not shown).

TABLE 2: Averages Calculated from the Trajectory Generated in the MD Simulation for the ψ_B^+ State of LNnT

C−H pair	S^2_{Ω}	H−H pair	S^2_{radial}	S^2_{Ω}	proton distance (Å)[a]
H1A−C1A	0.56	H1B−H3C	0.93	0.81	2.75
H4A−C4A	0.73	H1B−H4C	0.99	0.80	4.45
H3C−C3C	0.75	H4C−H3C	0.98	0.76	2.39
H4C−C4C	0.79	H4C−H5C	0.98	0.92	2.41

[a] $1/r = \langle r^{-6}\rangle^{1/6}$.

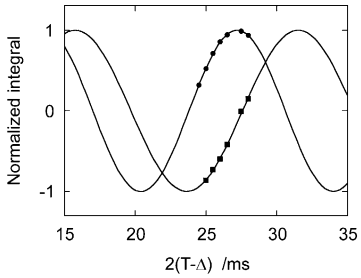

Figure 5. Intensity of the ^{1}H,^{13}C correlation for the H4−C4 pair in residue A as a function of the dephasing delay. The intensity profiles are shown as solid lines, and were fitted to experimental data in the isotropic (J, ●) and the ordered phase ($J + 2D$, ■).

We now turn to investigations of the liquid crystalline phases. The results from our previous studies of LNnT show that the shape of the molecule, to a first approximation, can be described as a prolate or an extended cylinder.[27] Moreover, the C−H bonds in LNnT can roughly be divided into two groups: vectors being either perpendicular or parallel to the principal axis of the molecule. However, in the previous analysis based on RDCs, the ^{13}C,^{1}H coupling at position 4 of residue C (Figure 1) exhibited a large fitting error. When LNnT was analyzed in two different lyotropic media, namely, DMPC/DHPC and cetylpyridinium chloride/*n*-hexanol/brine, a significant effect on this RDC was observed. The most conspicuous difference between the media is the larger salt concentration of the latter. Therefore, a sample of DMPC/DHPC in D_2O with 200 mM NaCl was prepared. However, the lyotropic phase was not stable during the ^{1}H,^{13}C HSQC experiment and the influence of salt could not be determined. This prompted a search for a lyotropic medium, which was compatible with higher salt concentrations. The C8E5/*n*-octanol/D_2O phase tolerates up to 500 mM NaCl and is still suitable for measurement of RDCs in biomolecules.[35] Thus, this phase was chosen as an appropriate medium to investigate the problems described above.

To utilize the RDCs from LNnT in the ordered phase with 200 mM NaCl and without salt, the *J*-modulated ^{1}H,^{13}C CT-HSQC experiment was used, which gives high precision in the measured data. A series of *J*-modulated intensity-based ^{1}H,^{13}C cross peaks for each resonance was fitted to the dephasing delay (Figure 5). The results for J and $J + 2D$ are shown in Table 3. The errors, analyzed by the jackknife procedure, are small. Likewise, the propagated errors from the two measurements in each of the two media used to obtain the RDCs are equally small (not shown). This is a prerequisite to be able to ascertain any difference for LNnT in the two media, whether of conformational origin or a change in the order tensor (or a combination thereof).

TABLE 3: Heteronuclear Spin−Spin and Dipolar Couplings (Hz) in LNnT (α-anomeric form) at 600 MHz in 5% C8E5/*n*-octanol/D_2O without Salt and with 200 mM NaCl

sugar residue	atom pair	water[a]		brine[b]	
		J	$J+2D$	J	$J+2D$
A	H1−C1	163.01 (0.08)[c]	182.82 (0.07)	163.06 (0.04)	182.22 (0.08)
A	H4−C4	147.04 (0.02)	126.90 (0.11)	147.13 (0.02)	128.44 (0.04)
B	H1−C1	163.52 (0.08)	183.81 (0.06)	163.53 (0.07)	183.06 (0.12)
B	H2−C2	143.70 (0.06)	165.49 (0.06)	143.95 (0.08)	164.13 (0.08)
C	H2−C2	144.58 (0.11)	167.70 (0.08)	144.86 (0.11)	165.82 (0.06)
C	H3−C3	138.27 (0.07)	161.19 (0.08)	138.96 (0.05)	159.14 (0.09)
C	H4−C4	149.62 (0.03)	134.15 (0.02)	149.53 (0.04)	135.07 (0.03)
D	H1−C1	170.06 (0.02)	150.94 (0.15)	170.18 (0.02)	152.42 (0.13)
D	H5−C5	145.95 (0.17)	165.05 (0.07)	146.24 (0.12)	163.64 (0.18)

[a] $\nu_Q = 39.4$ Hz. [b] $\nu_Q = 38.9$ Hz. [c] Standard deviation based on the jack-knife analysis procedure.

For most C−H pairs, the dipolar splitting differed by more than 1 Hz between the two media. For example, the H3−C3 interaction in residue C shows a difference of 2.7 Hz, which is an order of magnitude larger than the error. Furthermore, if no conformational change occurs for LNnT, then one should observe very similar dipolar couplings, considering the difference in the ^2H quadrupolar splitting for D_2O in the two media. Thus, the experimental results support the fact that the difference in the two media has a physical origin. Because the conformational change in LNnT is small, the difference in the RDCs between the two media indicates a variation of the ordering tensor.

To facilitate a quantitative analysis, the carbon−proton RDC can be expressed as

$$D_{CH} = -\frac{\mu_0}{8\pi^2}\frac{\gamma_C\gamma_H\hbar}{2}\langle(3\cos^2\theta - 1)r_{CH}^{-3}\rangle \qquad (1)$$

where r_{CH} is the spin−spin distance and θ is the angle between the spin−spin vector and the magnetic field. All other symbols have their usual meaning. To determine the orientation of the C−H vector in a molecular frame, we write eq 1 so it contains three successive rotations

$$D_{CH} = -\frac{\mu_0}{16\pi^2}\frac{\gamma_C\gamma_H\hbar}{r_{CH}^3}\kappa[S_{zz}(3\cos^2\theta_{CH}^z - 1) + (S_{xx} - S_{yy})(\cos^2\theta_{CH}^x - \cos^2\theta_{CH}^y)][3\cos^2\eta - 1] \qquad (2)$$

where κ is a scaling factor related to the order parameters and $\theta_{CH}^{\alpha}(\alpha = x, y, z)$ are the angles between the spin−spin vector and the molecular coordinate frame. The order parameters, $S_{\alpha\alpha}$, describe the second rotation: namely, the averaged transformation from the molecular axis system to the phase director. Finally, the angle η defines the orientation of the director with respect to the magnetic field ($\eta = 90°$). In the following, we assume that the molecular coordinate system, defined by the moment of inertia frame, coincides with the ordering tensor. Thus, the orientations of the C−H vectors in the molecular coordinate frame, that is, the angles θ_{CH}^{α} were determined from the trajectory generated in the MD computer simulations by calculating the moment of inertia tensor at every time step. A procedure for calculation of the order parameters, $S_{\alpha\alpha}$ ($\alpha = x, y, z$), from the eigenvalues of the inertia tensor, $I_{\alpha\alpha}$, was proposed for thermotropic liquid crystals[61] and rediscovered recently for weakly ordered phases.[62] In this approach, the order parameters are related to the molecular shape through the ellipsoid semiaxes, A_α, according to

$$S_{zz} = 1 - (A_x + A_y)/2A_z$$
$$S_{yy} = -1/2 + A_y/2A_z$$
$$S_{xx} = -1/2 + A_x/2A_z \qquad (3)$$

with

$$A_\alpha = [(I_{\beta\beta} + I_{\gamma\gamma} - I_{\alpha\alpha})5/2m]^{1/2} \qquad (4)$$

where m is the molecular mass. Conformational dependence of the (hypothetic) order parameters, $S_{\alpha\alpha}$, is shown in Figure 6. Clearly, the moment of inertia tensor and therefore the order parameters, in particular S_{zz}, are related to the transitions observed for the ψ_B torsion angle. In our analysis, eq 2 was numerically fitted to the experimental sets of dipolar couplings. A C−H distance of 1.117 Å was used,[63] and the fitting procedure was performed using a program based on the subroutine STEPIT.[64] The only free parameter used in the analysis was the scaling factor κ, which was adjusted to bring into agreement the calculated and experimental dipolar couplings. The scaling of the ordering tensor reflects the fact that the model used for calculation of the order parameters (eq 3) assumes that the average orientation is governed by the shape of the molecules forming the liquid crystal. This assumption is correct for neat liquid crystals formed by ellipsoidal molecules with semiaxes A_α. Notably, in dilute phases the order of the same molecule is considerably lower. The quality of the numerical fit was determined by

$$\text{error} = N^{-1}\sum_i \frac{|D_{CH}^i(\text{exptl}) - D_{CH}^i(\text{calcd})|}{|D_{CH}^i(\text{exptl})|} \qquad (5)$$

where D_{CH}^i is the dipolar coupling and N is the number of dipolar couplings. The analyses were carried out on the entire trajectory and on two fractions, each of 0.5 ns, corresponding to the two ψ_B states: ψ_B^+ and ψ_B^-. The relevant parameters are collected in Table 4, whereas the correlation between the experimental and calculated dipolar couplings is shown in Figure 7. We note that the correlation is significantly better (resulting in a smaller fitting error) for the ψ_B^+ state. However, the experimentally determined proton−proton distances cannot be explained using the ψ_B^+ state only; a mixture of the two states ψ_B^+ and ψ_B^- is required. A similar analysis was carried out employing a recently proposed model[10] in which the order parameters are calculated using the gyration tensor. The results of this analysis were essentially indistinguishable from those based on the inertia tensor, which is not surprising considering the fact that the coordinate frames of the two tensors coincide.[10]

To obtain additional information, we extracted proton−proton scalar ($^3J_{H,H}$) and residual dipolar couplings (D_{HH}) of LNnT from phase-sensitive COSY spectra, where the ordered phase cetylpyridinium chloride/*n*-hexanol/brine (200 mM NaCl in D_2O) was employed because of spectral distortion caused by the C8E5/*n*-octanol/D_2O phase. In LNnT we obtained $D_{HH} = 1.0$ Hz for H1A−H2A and $D_{HH} = 0.2$ Hz for H1C−H2C, assuming that $^3J_{H,H}$ are positive. The ordering of LNnT in the cetylpyridinium chloride/*n*-hexanol/brine phase is anticipated to be of a similar magnitude as that in the C8E5/*n*-octanol/D_2O phase,[23] thereby making it possible to employ the same value of κ in the analysis. Using the order tensor determined in the analysis of the ^1H,^{13}C RDCs together with the full trajectory (Table 4) the calculated D_{HH} couplings were 0.95 and 0.79 Hz, respectively. Considering

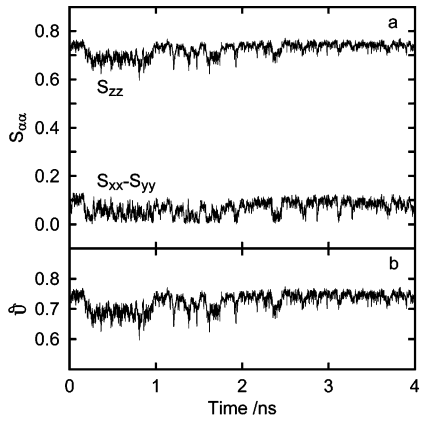

Figure 6. The time dependence of the (hypothetic) order parameters, $S_{\alpha\alpha}$, (a) and the generalized degree of order, ϑ, (b) in LNnT.

TABLE 4: Averages Calculated from the Trajectory Generated in the MD Simulation of LNnT

	conformational set		
parameter	ψ_B^+	ψ_B^-	full trajectory
I_{xx} (u·Å^2)	22 264	23 718	23 355
I_{yy} (u·Å^2)	23 594	25 734	25 012
I_{zz} (u·Å^2)	4190	3424	3659
S_{zz}	0.69	0.74	0.72
$S_{xx} - S_{yy}$	0.05	−0.09	0.07
κ	0.0014	0.0013	0.0014
error	0.12 (19)[a]	0.35 (146)	0.14 (32)

[a] Sum of squared errors in parentheses (in Hz^2).

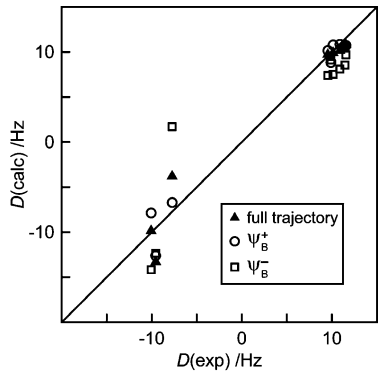

Figure 7. The correlation between observed and calculated NMR parameters for LNnT.

that the approximations and experimental errors were estimated to be ±0.5 Hz for the ACME procedure,[43] the agreement between calculated and experimental values is clearly acceptable. We note that the average angles, calculated from the MD trajectory, between the two H1−H2 spin−spin vectors and the long molecular axis are 67° and 64° for the A and C residues, respectively. These values are close to the "magic angle", which in turn makes the analysis extremely sensitive to the molecular biaxiality, $S_{xx} - S_{yy}$.

In our previous study of LNnT,[27] we analyzed the experimental dipolar couplings using trajectories, which were generated in several computer simulations employing different force fields. Some of the coupling sets produced large fitting errors, which indicated completely erroneous average conformations. We could therefore conclude, that some of the force fields were not suitable for simulations of carbohydrates. The force field used currently, however, is better than any of those reported previously, revealing an improved description of the conformational flexibility and dynamics of LNnT in the PARM22/SU01 force field.

Before closing this section, we comment on the frequently encountered problem related to the conformational dependence of the ordering tensor. A convenient scalar parameter that characterizes the molecular ordering is the generalized degree of order (GDO), ϑ[65]

$$\vartheta = \sqrt{\frac{2}{3}\sum_{\alpha\alpha} S_{\alpha\alpha}^2} \tag{6}$$

The advantage of the GDO concept is that it reflects both internal and orientational averaging and it can be expressed in any frame fixed in the molecule. In Figure 6, the time dependence of the GDO is demonstrated. Not surprisingly, the GDO closely mirrors the behavior of the principal order parameter, S_{zz}, and therefore the trajectory of the ψ_B torsion angle.

In a recent study, the influence of different liquid crystalline phases on the conformation of oligosaccharides was investigated.[66] Two mineral lyotropic phases were used to study the conformation of Lewis^x motif containing tri- and pentasaccharides. For the relatively rigid trisaccharide (defining the Lewis^x portion), structural consistency was observed between off-resonance ROESY data in water solution and RDCs in the two aligned media. In contrast, the conformational descriptors ϕ and ψ were found to differ for the pentasaccharide between the two media. It was concluded that interactions take place between the oligosaccharide and the mesogen and, consequently, the conformational equilibria are altered in the molecule. It is suggested that the conformational change takes place at the β-D-GlcNAc−(1 → 3)-D-Gal linkage in the pentasaccharide. Most interestingly with respect to this study, the structural elements of LNnT are found in the pentasaccharide and only three differences are present, namely, a methyl group, a sulfate group and a fucosyl group. Thus, the flexibility found for LNnT is also present in similar compounds and it is very important to ascertain when interactions with the alignment inducer also result in conformational changes.

Conclusions

In summary, we conclude that (a) the conformational flexibility described by the novel force field, resulting in a major and a minor conformation at the central glycosidic linkage, gives a better representation of LNnT in solution; (b) no significant salt effect is observed on the molecular structure of LNnT in the isotropic solution; and (c) only a minute salt effect is observed for the residual dipolar couplings that are oriented perpendicular to the principal axis, which leads to a slightly affected biaxiality of the ordering tensor. In view of the simple models used in the analyses of the RDCs, the conclusions provide a reasonable molecular picture of the oligosaccharide. In particular, the assumption about the ordering tensor coinciding with the moment of inertia frame strongly restricts the conformational information. Future studies on oligosaccharides in lyotropic crystalline media will utilize novel methodology[9,11] currently being developed in our laboratory to address complex issues of conformational dynamics.

Acknowledgment. This work was supported by grants from the Swedish Research Council (VR), the Carl Trygger Foundation, and the Swedish International Development Cooperation Agency (SIDA). We thank the Center for Parallel Computers, KTH, Stockholm, for putting computer facilities at our disposal and Dr. Alexandra Bernlind for stimulating discussions.

References and Notes

(1) Dong, R. Y. *Nuclear Magnetic Resonance of Liquid Crystals*; Springer: New York, 1994.

(2) Gaemers, S.; Bax, A. *J. Am. Chem. Soc.* **2001**, *123*, 12343−12352.

(3) Prestegard, J. H.; Al-Hashimi, H. M.; Tolman, H. M. *Q. Rev. Biophys.* **2000**, *33*, 371−424.

(4) Thompson, G. S.; Shimizu, H.; Homans, S. W.; Donohue-Rolfe, A. *Biochemistry* **2000**, *39*, 13153−13156.

(5) Gabriel, J.-C. P.; Camerel, F.; Lemaire, B. J.; Desvaux, H.; Davidson, P.; Batail, P. *Nature* **2001**, *413*, 504−508.

(6) Schulte-Herbrüggen, T.; Untidt, T. S.; Nielsen, N. C.; Sørensen, O. W. *J. Chem. Phys.* **2001**, *115*, 8506−8517.

(7) Pham, T. N.; Liptaj, T.; Bromek, K.; Uhrín, D. *J. Magn. Reson.* **2002**, *157*, 200−209.

(8) Pham, T. N.; Liptaj, T.; Barlow, P. N.; Uhrín, D. *Magn. Reson. Chem.* **2002**, *40*, 729−732.

(9) Stevensson, B.; Landersjö, C.; Widmalm, G.; Maliniak, A. *J. Am. Chem. Soc.* **2002**, *124*, 5946−5947.

(10) Almond, A.; Axelsen, J. B. *J. Am. Chem. Soc.* **2002**, *124*, 9986−9987.

(11) Stevensson, B.; Sandström, D.; Maliniak, A. *J. Chem. Phys.* **2003**, *119*, 2738−2746.

(12) Valafar, H.; Prestegard, J. H. *J. Magn. Reson.* **2004**, *167*, 228−241.

(13) Ramirez, B. E.; Bax, A. *J. Am. Chem. Soc.* **1998**, *120*, 9106−9107.

(14) Peti, W.; Meiler, J.; Brüschweiler, R.; Griesinger, C. *J. Am. Chem. Soc.* **2002**, *124*, 5822−5833.

(15) Tolman, J. R. *J. Am. Chem. Soc.* **2002**, *124*, 12020−12030.

(16) Meiler, J.; Peti, W.; Griesinger, C. *J. Am. Chem. Soc.* **2003**, *125*, 8072−8073.

(17) Koenig, B. W.; Hu, J.-S.; Ottiger, M.; Bose, S.; Hendler, R. W.; Bax, A. *J. Am. Chem. Soc.* **1999**, *121*, 1385−1386.

(18) Sass, J.; Cordier, F.; Hoffmann, A.; Rogowski, M.; Cousin, A.; Omichinski, J. G.; Löwen, H.; Grzesiek, S. *J. Am. Chem. Soc.* **1999**, *121*, 2047−2055.

(19) Staaf, M.; Höög, C.; Stevensson, B.; Maliniak, A.; Widmalm, G. *Biochemistry* **2001**, *40*, 3623−3628.

(20) Neubauer, H.; Meiler, J.; Peti, W.; Griesinger, C. *Helv. Chim. Acta* **2001**, *84*, 243−258.

(21) Tian, F.; Al-Hashimi, H. M.; Craighead, J. L.; Prestegard, J. H. *J. Am. Chem. Soc.* **2001**, *123*, 485−492.

(22) Almond, A.; Bunkenborg, J.; Franch, T.; Gotfredsen, C. H.; Duus, J. Ø. *J. Am. Chem. Soc.* **2001**, *123*, 4792−4802.

(23) Lycknert, K.; Maliniak, A.; Widmalm, G. *J. Phys. Chem. A* **2001**, *105*, 5119−5122.

(24) Manuel-Pastor, M.; Canales, A.; Corzana, F.; Asensio, J. L.; Jiménez-Barbero, J. *J. Am. Chem. Soc.* **2005**, *127*, 3589−3595.

(25) Kunz, C.; Rudloff, S.; Baier, W.; Klein, N.; Strobel, S. *Annu. Rev. Nutr.* **2000**, *20*, 699−722.

(26) Rundlöf, T.; Landersjö, C.; Lycknert, K.; Maliniak, A.; Widmalm, G. *Magn. Reson. Chem.* **1998**, *36*, 773−776.

(27) Landersjö, C.; Höög, C.; Maliniak, A.; Widmalm, G. *J. Phys. Chem. B* **2000**, *104*, 5618−5624.

(28) Manuel-Pastor, M.; Bush, C. A. *Carbohydr. Res.* **2000**, *323*, 147−155.

(29) Manuel-Pastor, M.; Bush, C. A. *Biochemistry* **2000**, *39*, 4674−4683.

(30) Manuel-Pastor, M.; Bush, C. A. *J. Biomol. NMR* **2001**, *19*, 125−139.

(31) Azurmendi, H. F.; Manuel-Pastor, M.; Bush, C. A. *Biopolymers* **2002**, *63*, 89−98.

(32) Almond, A.; Petersen, B. O.; Duus, J. Ø. *Biochemistry* **2004**, *43*, 5853−5863.

(33) Moran, A. P.; Prendergast, M. M.; Appelmelk, B. J. *FEMS Immunol. Med. Microbiol.* **1996**, *16*, 105−115.

(34) Penders, M. H. G. M.; Strey, R. *J. Phys. Chem.* **1995**, *99*, 6091−6095.

(35) Rückert, M.; Otting, G. *J. Am. Chem. Soc.* **2000**, *122*, 7793−7797.

(36) Kjellberg, A.; Widmalm, G. *Biopolymers* **1999**, *50*, 391−399.

(37) Nishida, T.; Widmalm, G.; Sándor, P. *Magn. Reson. Chem.* **1996**, *34*, 377−382.

(38) Tjandra, N.; Bax, A. *J. Magn. Reson.* **1997**, *124*, 512−515.

(39) Mosteller, F.; Tukey, J. W. *Data Analysis and Regression. A Second Course in Statistics*; Addison-Wesley: Reading, MA, 1977.

(40) Evenäs, J.; Mittermaier, A.; Yang, D.; Kay, L. E. *J. Am. Chem. Soc.* **2001**, *123*, 2858−2864.

(41) Miller, J. C.; Miller, J. N. *Statistics for Analytical Chemistry*, 3rd ed.; Ellis Horwood: New York, 1993.

(42) Delaglio, F.; Grzesiek, S.; Vuister, G. W.; Zhu, G.; Pfeifer, J.; Bax, A. *J. Biomol. NMR* **1995**, *6*, 277−293.

(43) Delaglio, F.; Wu, Z.; Bax, A. *J. Magn. Reson.* **2001**, *149*, 276−281.

(44) Brooks, B. R.; Bruccoleri, R. E.; Olafson, B. D.; States, D. J.; Swaminathan, S.; Karplus, M. *J. Comput. Chem.* **1983**, *4*, 187−217.

(45) MacKerell, A. D., Jr.; Bashford, D.; Bellott, M.; Dunbrack, R. L., Jr.; Evanseck, J. D.; Field, M. J.; Fischer, S.; Gao, J.; Guo, H.; Ha, S.; Joseph-McCarthy, D.; Kushnir, L.; Kuczera, K.; Lau, F. T. K.; Mattos, C.; Michnick, S.; Ngo, T.; Nguyen, T. D.; Prodhom, B.; Reiher, W. E., III; Roux, B.; Schlenkrich, M.; Smith, J. C.; Stote, R.; Straub, J.; Watanabe, M.; Wiórkiewicz-Kuczera, J.; Yin, D.; Karplus, M. *J. Phys. Chem. B* **1998**, *102*, 3586−3616.

(46) Eklund, R.; Widmalm, G. *Carbohydr. Res.* **2003**, *338*, 393−398.

(47) Neria, E.; Fischer, S.; Karplus, M. *J. Chem. Phys.* **1996**, *105*, 1902−1921.

(48) Hockney, R. W. *Methods Comput. Phys.* **1970**, *9*, 136−211.

(49) Ryckaert, J. P.; Ciccotti, G.; Berendsen, H. J. C. *J. Comput. Phys.* **1977**, *23*, 327−341.

(50) Berendsen, H. J. C.; Postma, J. P. M.; van Gunsteren, W. F.; DiNola, A.; Haak, J. R. *J. Chem. Phys.* **1984**, *81*, 3684−3690.

(51) Steinbach, P. J.; Brooks, B. R. *J. Comput. Chem.* **1994**, *15*, 667−683.

(52) Hwang, T.-L.; Shaka, A. J. *J. Magn. Reson., Ser. B* **1993**, *102*, 155−165.

(53) *The Anomeric Effect and Associated Stereoelectronic Effects*; Thatcher, G. R., Ed.; American Chemical Society: Washington, DC, 1993; ACS Symp. Ser. 539.

(54) Cloran, F.; Carmichael, I.; Serianni, A. S. *J. Am. Chem. Soc.* **1999**, *121*, 9843−9851.

(55) Widmalm, G.; Pastor, R. W. *J. Chem. Soc., Faraday Trans.* **1992**, *88*, 1747−1754.

(56) Pastor, R. W. In *The Molecular Dynamics of Liquid Crystals*; Luckhurst, G. R., Veracini, C. A., Eds.; Kluwer Academic Publishers: Dordrecht, The Netherlands, 1994; pp 85−138.

(57) Dixon, A. M.; Venable, R. M.; Widmalm, G.; Bull, T. E.; Pastor, R. W. *Biopolymers* **2003**, *69*, 448−460.

(58) Lipari, G.; Szabo, A. *J. Am. Chem. Soc.* **1982**, *104*, 4546−4559.

(59) Brüschweiler, R.; Roux, B.; Blackledge, M.; Griesinger, C.; Karplus, M.; Ernst, R. R. *J. Am. Chem. Soc.* **1992**, *114*, 2289−2302.

(60) Rundlöf, T.; Venable, R. M.; Pastor, R. W.; Kowalewski, J.; Widmalm, G. *J. Am. Chem. Soc.* **1999**, *121*, 11847−11854.

(61) Samulski, E. T.; Dong, R. Y. *J. Chem. Phys.* **1982**, *77*, 5090−5096.

(62) Azurmendi, H. F.; Bush, C. A. *J. Am. Chem. Soc.* **2002**, *124*, 2426−2427.

(63) Ottiger, M.; Bax, A. *J. Am. Chem. Soc.* **1998**, *120*, 12334−12341.

(64) Chandler, J. P. Program no. 307, QCPE, Chemistry Department, Indiana University, Bloomington, IN 47405, 1982.

(65) Tolman, J. R.; Al-Hashimi, H. M.; Kay, L. E.; Prestegard, J. H. *J. Am. Chem. Soc.* **2001**, *123*, 1416−1424.

(66) Berthault, P.; Jeannerat, D.; Camerel, F.; Salgado, F. A.; Boulard, Y.; Gabriel, J.-C. P.; Desvaux, H. *Carbohydr. Res.* **2003**, *338*, 1771−1785.